Dual amyloid domains promote differential functioning of the chaplin proteins during *Streptomyces* aerial morphogenesis

David S. Capstick[a], Ahmad Jomaa[b], Chistopher Hanke[a], Joaquin Ortega[b], and Marie A. Elliot[a,1]

[a]Department of Biology and M.G. DeGroote Institute for Infectious Disease Research, McMaster University, 1280 Main Street West, Hamilton, ON, Canada L8S 4K1; and [b]Department of Biochemistry and Biomedical Sciences and M.G. DeGroote Institute for Infectious Disease Research, McMaster University, 1200 Main Street West, Hamilton, ON, Canada L8N 3Z5

Edited by David S. Eisenberg, University of California, Los Angeles, CA, and approved May 6, 2011 (received for review December 15, 2010)

The chaplin proteins are functional amyloids found in the filamentous *Streptomyces* bacteria. These secreted proteins are required for the aerial development of *Streptomyces coelicolor*, and contribute to an intricate rodlet ultrastructure that decorates the surfaces of aerial hyphae and spores. *S. coelicolor* encodes eight chaplin proteins. Previous studies have revealed that only three of these proteins (ChpC, ChpE, and ChpH) are necessary for promoting aerial development, and of these three, ChpH is the primary developmental determinant. Here, we show that the model chaplin, ChpH, contains two amyloidogenic domains: one in the N terminus and one in the C terminus of the mature protein. These domains have different polymerization properties as determined using fluorescence spectroscopy, secondary structure analyses, and electron microscopy. We coupled these in vitro assays with in vivo genetic studies to probe the connection between ChpH amyloidogenesis and its biological function. Using mutational analyses, we demonstrated that both N- and C-terminal amyloid domains of ChpH were required for promoting aerial hypha formation, while the N-terminal domain was dispensable for assembly of the rodlet ultrastructure. These results suggest that there is a functional differentiation of the dual amyloid domains in the chaplin proteins.

Streptomyces development | sporulation | surface ultrastructure

Amyloid proteins are associated with a number of diseases including Alzheimer's and type 2 diabetes. These proteins aggregate to form insoluble β-sheet-rich fibers that are resistant to proteolytic degradation and accumulate as amyloid plaques. Recently, a new class of functional amyloids has emerged, which have evolved to circumvent the toxicity traditionally associated with amyloid formation. These functional amyloids are found in a wide range of organisms and have a diverse array of functions (1). In bacteria, amyloids can act as toxins and virulence factors (2, 3), and can also mediate cell adhesion and biofilm formation, as seen for MTP (*Mycobacterium tuberculosis*), TasA (*Bacillus subtilis*), HfaA (*Caulobacter crescentus*), FapC (*Pseudomonas* sp.), and curli/tafi (*Escherichia coli*/*Salmonella*) (4–8). The chaplins, a family of eight secreted proteins (ChpA-H) produced by the filamentous bacterium *Streptomyces coelicolor*, are another example of amyloidogenic proteins involved in cell attachment (9). The chaplins are, however, multifunctional proteins, in that they also promote cellular differentiation in *S. coelicolor* during growth on solid culture, and alter the surface characteristics of cells in the later stages of development (10–12).

The *Streptomyces* life cycle encompasses three distinct cell types: branching vegetative hyphae, aerial hyphae which emerge from the vegetative cells, and spore chains which develop in the aerial hyphae (13). The chaplins are proposed to mediate the raising of aerial hyphae by lowering surface tension at the aqueous colony surface (12). These proteins work in concert with SapB, a lantibiotic-like peptide (14), during growth in nutrient-rich conditions, but when nutrients are limiting, aerial development is exclusively chaplin-dependent (10). With the exception of ChpE, all chaplin domains contain two highly conserved cysteine (Cys) residues that form intramolecular disulfide bonds (15). The chaplins can be divided into two groups: the short chaplins (ChpD-H) and the long chaplins (ChpA-C), where the long chaplins have a C-terminal sorting signal that likely targets them for cell wall attachment. On the cell surface, the short chaplins polymerize into fibers that are predicted to interact with the cell-wall-anchored long chaplins (11, 12). Chaplin fibers decorate the surface of aerial hyphae and spores, adopting a paired-rod (rodlet) ultrastructure. This rodlet organization also requires the activity of the rodlin proteins, RdlA and RdlB (16, 17). The chaplin/rodlin fibers provide a resilient hydrophobic coat that may protect against desiccation and provide stability to aerial structures. Chaplin fibers are rich in β-sheet secondary structure, are highly insoluble, and readily bind the amyloid-specific dyes Congo red and thioflavin T (ThT) (9, 12). How the chaplins form amyloid fibers and what is required for their polymerization is not known.

Amyloid-forming proteins frequently contain one or more amyloid domains. These domains are short stretches of sequence that drive amyloidogenesis, forming amyloid fibers in vitro and promoting amyloidogenesis in vivo (18, 19). We predicted that the chaplins would have one or more amyloid sequence determinants. To investigate chaplin amyloidogenesis, we focused our studies on ChpH. Of the chaplins produced by *S. coelicolor*, only ChpC, ChpE, and ChpH are conserved across *Streptomyces* species, and we previously showed that a "minimal chaplin strain" encoding only these chaplins could raise a robust aerial mycelium (15). In this minimal background, ChpH was the major contributor to aerial hypha formation. Here, we show that ChpH has two amyloid domains, an N- and C-terminal domain, with each having different polymerization characteristics. Both domains are necessary for promoting the aerial development of *S. coelicolor*, but the C-terminal domain appears to be more important for rodlet assembly than the N-terminal domain.

Results

In Vitro Characterization of ChpH Amyloidogenesis. To investigate ChpH amyloid fiber formation, we used a synthetic 49 amino acid (aa) peptide that corresponded to the mature ChpH sequence (Fig. 1). We followed amyloid fiber formation using the amyloid-specific dye ThT (20), and observed a large increase in fluorescence over 24 h, after which levels plateaued (Fig. 2*A*). There was

Author contributions: D.S.C. and M.A.E. designed research; D.S.C., A.J., and C.H. performed research; D.S.C. contributed new reagents/analytic tools; D.S.C., A.J., J.O., and M.A.E. analyzed data; and D.S.C., J.O., and M.A.E. wrote the paper.

The authors declare no conflict of interest.

This article is a PNAS Direct Submission.

[1]To whom correspondence should be addressed. E-mail: melliot@mcmaster.ca.

This article contains supporting information online at www.pnas.org/lookup/suppl/doi:10.1073/pnas.1018715108/-/DCSupplemental.

BIOCHEMISTRY

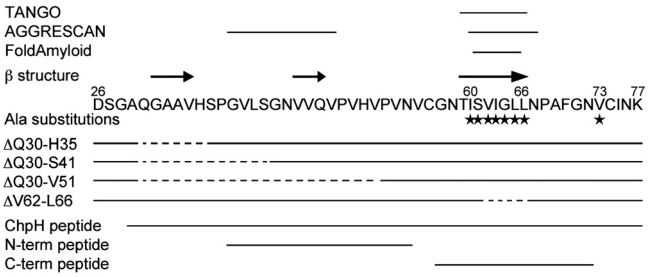

Fig. 1. Sequence of the mature ChpH protein. (*Top to bottom*) Amyloidogenic/aggregation-prone regions (marked by solid lines) predicted by the indicated programs. Sequences predicted to adopt β secondary structure (arrows). Mutagenesis of ChpH: Ala substitutions (stars) and deletions (dashed lines). Synthetic peptides used to analyze the N- and C-terminal amyloid domains (solid lines).

no obvious lag phase, irrespective of ChpH peptide concentration tested (Fig. 2*A*, inset); however, seeding of this reaction using three different ChpH amyloid preparations reproducibly accelerated amyloid fiber formation to varying degrees (Fig. 2*B*). Secondary structural analysis using circular dichroism (CD) spectroscopy revealed ChpH to be initially unstructured, but over 24 h it became increasingly β-rich (Fig. 2*C*). To observe ChpH amyloid fiber morphology, we used negative staining electron microscopy (EM). After a 24 h incubation, we observed primarily large, dense tangles of fibers (Fig. 2*D*), although individual fibers and smaller aggregates were seen occasionally (Fig. S1). The distribution and appearance of fibers did not change noticeably over time (Fig. S2). ChpH fibers typically exhibited a twisted conformation, and when outside of the large clusters, they were frequently wrapped around each other (Fig. S1). To further validate the amyloid nature of these fibers, we tested them for resistance to Proteinase K; they retained their β-rich characteristics under conditions when other proteins lost any semblance of structure (Fig. S3). Collectively, these results show that ChpH can readily form amyloid fibers in vitro.

The C Terminus of ChpH Is Amyloidogenic. We predicted there to be one or more regions responsible for driving ChpH amyloidogenesis. To identify these sequences, we took an *in silico* approach, analyzing the ChpH sequence using programs that predict amyloidogenic or aggregation-prone regions: Tango (21), AGGRESCAN (22), and FoldAmyloid (23). While each program predicted slightly different amyloidogenic/aggregation-prone sequences within ChpH, the same five aa (SVIGL) in the C terminus were identified by all (Fig. 1). To test these predictions, a nine aa peptide (TISVIGLLN) was synthesized and assessed for its ability to form amyloid fibers. This peptide did not reproducibly bind ThT, and failed to exhibit β secondary structure, even after extended (12 d) incubation, as determined using CD spectroscopy. We hypothesized that the neighboring sequence context was important, as the SVIGL sequence was within a region constrained by a disulfide bridge (11). To investigate this possibility, we used a 16 aa peptide spanning the region between the bridging Cys residues (GNTISVIGLLNPAFGN) (Fig. 1). This peptide bound significant amounts of ThT, although its binding kinetics were different from that of the full length ChpH (Fig. 3*A*). There was an initial 24 h lag before fluorescence increased dramatically. This increase was then reproducibly followed by a precipitous drop in fluorescence at 96 h. Examining the peptide structure over time using CD spectroscopy revealed a transition to β secondary structure within 24 h, and an increase in β structure over the next 72 h (Fig. 3*B*). The seeding experiments in Fig. 2*B* also showed that sonicated 120 h fibers could effectively promote full length ChpH polymerization. These analyses suggested that the drop in ThT fluorescence at 96 h was unlikely to be due to fiber disaggregation, and instead could be the result of changes in fiber associations that limit ThT binding. The latter hypothesis was supported by our observations of peptide morphology using negative staining EM. At 72 h, the C-terminal peptide had formed thin, straight fibers that assembled into tangled networks (Fig. 3*C*). By 96 h, however, these fiber networks were no longer observed, and instead, only individual aggregates (single fibers twisted around each other) could be detected (Fig. 3*D*), and by 120 h, these aggregates had become shorter and thicker (Fig. S2). We tested the resistance of these fibers to Proteinase K and found that, like for the full length ChpH, they were resis-

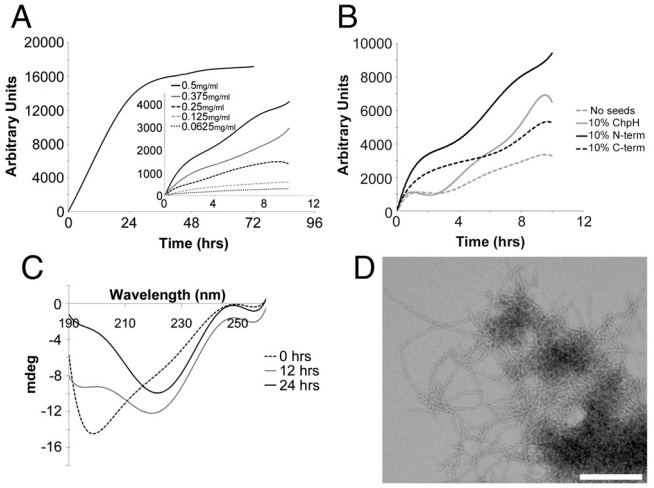

Fig. 2. In vitro polymerization of the full length ChpH peptide. (*A*) ThT fluorescence induced by ChpH (0.5 mg/mL) over 72 h (readings taken at 24 h intervals). Inset: ThT fluorescence of ChpH at different concentrations (readings taken every 10 min for 10 h). (*B*) ThT fluorescence of ChpH (0.5 mg/mL) alone, or in the presence of 10% (w/w) sonicated ChpH, C-terminal or N-terminal fibers, over 10 h (readings taken every 10 min). (*C*) CD analysis of ChpH (diluted from 0.5 to 0.25 mg/mL) before incubation and after incubating for 12 and 24 h. (*D*) Negatively stained electron micrograph of a ChpH peptide solution (0.5 mg/mL) incubated at room temperature for 120 h. (Scale bar, 250 nm).

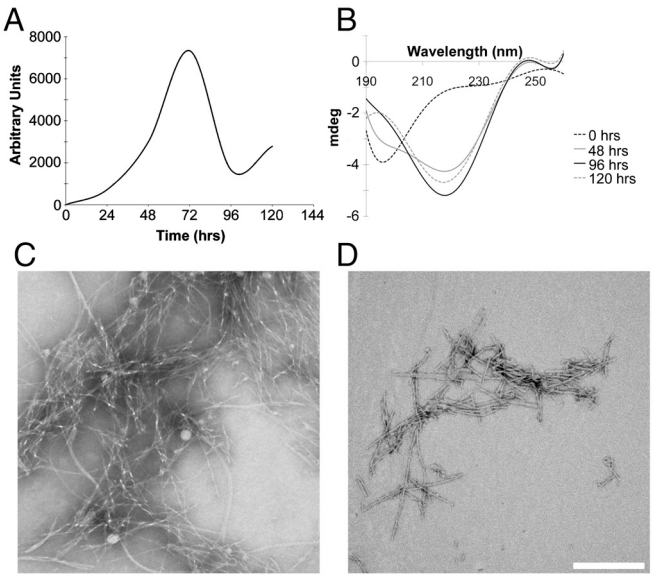

Fig. 3. In vitro polymerization of the C-terminal ChpH peptide (GNTISVIGLLNPAFGN). (*A*) ThT fluorescence of the peptide (0.5 mg/mL) over 120 h (24 h intervals). (*B*) CD analysis of the peptide (diluted from 0.5 to 0.25 mg/mL) from 0 to 120 h. (*C*–*D*) Negatively stained electron micrographs of the peptide (0.5 mg/mL) incubated at room temperature for (*C*) 72 h or (*D*) 96 h. (Scale bar, 250 nm).

tant to degradation (Fig. S3). Taken together, these results show that the C terminus of ChpH contains an amyloid domain, and that it can undergo higher order structural changes.

In Vitro Characterization of ChpH Mutants. Given the amyloid characteristics exhibited by the 16 aa C-terminal peptide, we were interested in probing the importance of the predicted aggregation-prone sequence (Fig. 1). In particular, we wanted to determine whether this region was the major amyloidogenicity determinant, or whether additional sequences in this peptide were important for amyloid formation, given that the 16 aa peptide exhibited classical amyloid characteristics, whereas the 9 aa peptide (containing the predicted aggregative sequence) did not. To explore the functional importance of this region in ChpH, we tested two mutant derivatives of the C-terminal peptide: one harboring a V62A point mutation (GNTIS**A**IGLLNPAFGN) and the other replacing the central VIGLL sequence with five alanine residues (GNTIS**AAAAA**NPAFGN). Both mutant peptides yielded very little fluorescence when mixed with ThT, even after 120 h of incubation. A 10-fold increase in peptide concentration led to modest fluorescence of the V62A peptide (peaking at ~2,000 relative fluorescence units), but no increase was observed for the VIGLL-AAAAA peptide (Fig. S4). Both peptides failed to adopt any detectable β secondary structure, as determined by CD analysis, remaining unstructured for up to 16 d after initiating incubation, irrespective of peptide concentration (Fig. S4). We were, however, able to detect fibers for both peptides using negative staining EM: V62A mutant fibers were rare at 0.5 mg/mL but were more abundant at 5 mg/mL, while the VIGLL-AAAAA mutant fibers were sparse and difficult to find, even at 5 mg/mL (Fig. S4). The mutant fibers differed from those of the wild type C-terminal peptide: the V62A peptide produced short, straight, needle-like fibers with a low tendency to bundle or associate into fiber networks, while the VIGLL-AAAAA peptide formed occasional thin, curved fibers (Fig. S4). The fibers observed for each mutant peptide may be protein aggregates and not amyloids, given the lack of detectable ThT fluorescence or β-secondary structure for either. We could not, however, exclude the possibility that amyloid fibers constitute a small proportion of the overall peptide composition, and that the secondary structure and fluorescent analyses, which are concentration dependent, failed to detect them. Irrespective, amyloid fiber formation is, at best, severely compromised for both mutant peptides when compared with the wild type C-terminal peptide.

Amyloidogenesis of ChpH Is Required for Promoting Aerial Development. In vivo, ChpH has an important developmental role, contributing to the morphological differentiation of *Streptomyces*. To explore the significance of the ChpH C-terminal amyloid domain in vivo, and establish a structure-function relationship, we conducted scanning Ala mutagenesis of this region (Fig. 1). We also mutagenized several residues outside of the amyloid domain (I60A and V73A). Each mutant *chpH* gene (*chpH**) was cloned in place of wild type *chpH*, directly upstream of *chpC* in an integrating plasmid vector (*chpC* and *chpH* are found adjacent to each other in all streptomycete genomes). The resulting constructs were introduced into a strain where all chaplins apart from *chpE* had been deleted, reconstituting the minimal chaplin strain. These strains were then visually screened for developmental defects during colony formation. Because wild type ChpH function is essential for aerial hypha formation by the minimal chaplin strain (15), mutants with impaired ChpH function could be readily identified by their inability to raise a robust aerial mycelium. After 5 d, strains expressing I60A and V73A substituted ChpH (residues outside of the predicted "SVIGL" amyloidogenic region) behaved like the strain expressing wild type *chpH*, appearing light gray (indicative of aerial hyphae). In contrast, the S61A, V62A, I63A, G64A, L65A, and L66A ChpH-expressing strains

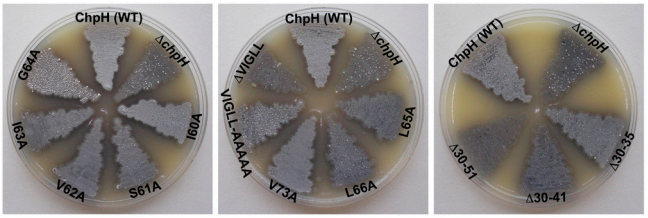

Fig. 4. 120 h cultures grown on MS medium, expressing wild type (WT) ChpH, lacking ChpH (Δ*chpH*), and expressing mutant ChpH proteins bearing amino acid substitutions or deletions.

were compromised in their ability to raise aerial hyphae, as seen by their darker (vegetative) coloration (Fig. 4); the white dots speckling the surface of some strains likely represent suppressor mutants. Notably, each of the ChpH substitutions that affected development was within, or immediately adjacent to, the SVIGL "amyloid domain" sequence, underscoring the importance of this region for ChpH function.

The developmental phenotype observed for the Ala mutants could be due to reduced protein stability, mislocalization of the mutant ChpH proteins, or defective protein function. To differentiate between these possibilities, we isolated chaplins from the aerial surfaces of mutant strains and analyzed them using MALDI-ToF mass spectrometry. The mutant proteins were effectively secreted and present in normal abundance, using ChpE levels for relative comparison (Fig. S5). These results implied that the defective development by the *chpH** mutants was not due to defects in ChpH* localization or stability, but rather inefficient amyloid fiber formation by the mutant ChpH proteins.

Given that Ala substitutions within the predicted amyloid domain adversely affected development, we tested the effect of deleting this region altogether. The effect was severe: by day 5, this strain could raise only a very sparse aerial mycelium, and most closely resembled a mutant lacking *chpH* (Fig. 4). We worried that this deletion may impact ChpH structure, given the constraints imposed by the flanking disulfide bridge, so we also replaced each of the five deleted amino acids with Ala residues, to retain the aa number found in wild type ChpH. After 5 d, the resulting mutant most closely resembled the single Ala mutants. However, after 12 d, scanning electron microscopy (SEM) revealed that the VIGLL-AAAAA mutant, along with the Δ*chpH* strain, had failed to develop abundant spore chains (5–10 fold fewer than a strain expressing wild type ChpH), whereas a V62A mutant appeared wild type in terms of spore abundance (Fig. S6). We determined that both VIGLL-AAAAA and ChpH(ΔVIGLL) mutant proteins were cell-surface localized and present in wild type abundance using MALDI-ToF analysis, verifying that the observed phenotypes were not due to defective secretion or stability (Fig. S5).

Perturbation of ChpH activity can inhibit not only the raising of aerial hyphae, but also rodlet ultrastructure assembly on aerial surfaces (15). Using SEM, we examined aerial hyphae and spores of select ChpH mutants to determine whether these mutations influenced surface architecture. As seen previously (15), the spores of strains expressing wild type ChpH were covered with abundant surface fibers arranged in pairs or bundles (Fig. 5). In comparison, the Δ*chpH* mutant surface exhibited markedly fewer fibers (Fig. 5). Of the ChpH mutant strains examined, the VIGLL-AAAAA mutant had the greatest impairment in surface architecture, producing occasional fibers sparsely distributed over the aerial surfaces, and appearing most similar to the Δ*chpH* mutant. In contrast, the V62A mutant surface most closely resembled that of the wild type ChpH-expressing strain (Fig. 5).

The N Terminus of ChpH Contains a Second Amyloid Domain and Is Critical for ChpH Function. Our results strongly support a C-terminal amyloid domain for ChpH, and our in vivo analyses further

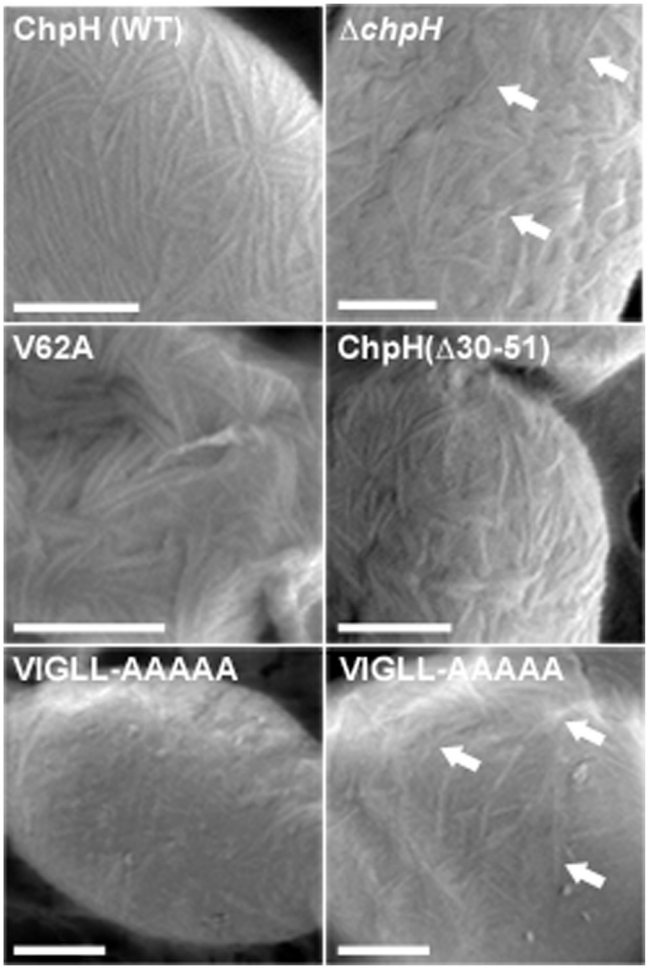

Fig. 5. SEM micrographs focused on the surface ultrastructure of a strain producing wild type (WT) ChpH, lacking ChpH (Δ*chpH*), and three strains expressing different mutant ChpH proteins. (Scale bars, 200 nm). For strains showing little ultrastructure, arrows point to occasional fibers on the aerial surfaces.

support a role for this sequence in both promoting aerial hypha formation and assembling a rodlet ultrastructure. We were therefore interested in determining whether the N terminus of ChpH was dispensable for function. Secondary structural analyses suggested this region was β-strand rich (Fig. 1) (24, 25), and the AGGRESCAN program (22) predicted aggregative properties for a 10 aa sequence within this region (Fig. 1). To probe the in vivo function of this region, we generated three N-terminal deletions (Fig. 1) and introduced each deletion construct into the minimal chaplin strain in place of wild type *chpH*. Deleting six aa (the first β-strand, $\Delta ChpH_{30–35}$) had no obvious impact on aerial development (Fig. 4), while deleting 12 and 22 aa ($\Delta ChpH_{30–41}$ and $\Delta ChpH_{30–51}$; Fig. 1) led to significant developmental defects (Fig. 4). The 12 aa deletion removed the first β-strand, as well as the first four residues of the predicted aggregative sequence, and the phenotypic effect was most similar to that of the C-terminal Ala substitution mutants. In contrast, the 22 aa deletion, which removed both β-strands and the entire predicted aggregative sequence, led to a defect that was as severe as that conferred by the C-terminal ΔVIGLL and the Δ*chpH* mutation (Fig. 4, Fig. S6). This deletion did not impact ChpH secretion, localization, or abundance (Fig. S5). The impaired aerial development of the two N-terminal deletion strains suggested these sequences were important for ChpH function. When we examined the aerial surface of the $\Delta ChpH_{30–51}$ (22 aa deletion) mutant, we found it to have a similar ultrastructure to that of the V62A mutant, forming relatively abundant fibers (Fig. 5), suggesting that while the N terminus of ChpH was critical for promoting aerial hyphae formation, it was dispensable for rodlet assembly.

To investigate the amyloidogenic potential of the N terminus, we generated a synthetic 17 aa peptide containing the second predicted amyloid domain (GVLSGNVVQVPVHVPVN) (Fig. 1). This peptide effectively bound ThT with a reproducible biphasic fluorescence profile (Fig. 6*A*), and could robustly seed the polymerization of full length ChpH fibers (Fig. 2*B*). These characteristics suggested it had a major role in promoting ChpH amyloid formation. Structural analyses suggested that this peptide began adopting β-structure by 24 h, and became more structured over time (Fig. 6*B*). Interestingly, the N-terminal peptide fiber morphology was unique: negatively stained electron micrographs revealed long, straight filament bundles (Fig. 6*C*, Fig. S1) that did not associate further into the three-dimensional tangles seen for the other wild type ChpH peptides. This morphology did not change significantly over time (Fig. S2). We tested the ability of these fibers to withstand protease treatment, and like the others, they were resistant to the effects of Proteinase K (Fig. S3). Our results, therefore, show that ChpH has two independent amyloidogenic regions, with each being sufficient to induce amyloid fiber formation, but both apparently being required to produce the dense polymers observed for the mature ChpH.

Discussion

The chaplins are members of a growing class of functional amyloids (26). Until now, there has been little understood about the sequences responsible for chaplin amyloid formation, and the extent to which the chaplin amyloid properties contributed to their morphogenetic function. Here, we provide direct evidence linking chaplin amyloid formation to aerial development, and identify two amyloid domains that contribute differentially to the functioning of ChpH.

Amyloid formation is often promoted by short contiguous sequences within a larger protein context (18, 19). Both ChpH amyloid domains correspond to regions predicted to adopt β-strands; a third predicted β-strand at the extreme N terminus

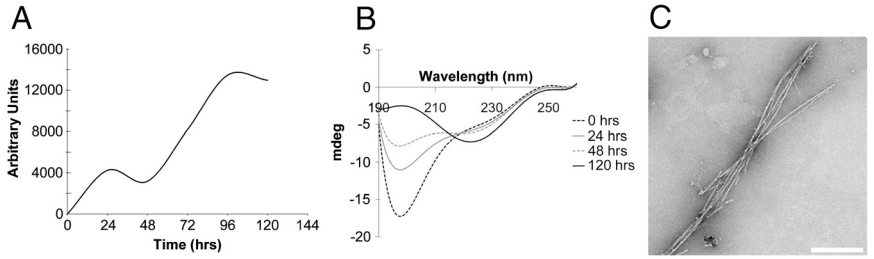

Fig. 6. In vitro polymerization of the N-terminal ChpH peptide (GVLSGNVVQVPVHVPVN). (*A*) ThT fluorescence of the peptide (0.5 mg/mL) over 120 h (24 h intervals). (*B*) CD analysis of the peptide (diluted from 0.5 mg/mL to 0.25 mg/mL) from 0 to 120 h. (*C*) Negatively stained electron micrographs of the peptide (0.5 mg/mL) incubated for 120 h at room temperature. (Scale bar, 250 nm).

of the mature protein was not required for ChpH activity. The chaplins are not unique in having multiple amyloid domains. The curli protein CsgA from *E. coli* contains several amyloidogenic domains: at least three domains can form amyloids in vitro, but only two are critical for in vivo amyloid formation (27, 28). A similar architecture has been observed for the type II diabetes-associated amyloid, human islet amyloid polypeptide (hIAPP). This peptide has three amyloid domains (29–31), with each domain containing a predicted β-strand. While discrete functions have not been ascribed to the different curli amyloid domains, the N terminus of hIAPP (amyloid domain 1) can disrupt membrane activity, suggesting that there may be functional differentiation of the domains in hIAPP. A similar situation exists for ChpH, where both amyloid domains are required for aerial hypha formation, but the C-terminal domain makes a greater contribution to rodlet assembly. This functional specialization is further reflected in the different polymerization and morphological features exhibited by each domain in vitro (Fig. S1).

Amyloids typically assemble into polymers though a nucleation-dependent process. Nucleation-dependent assembly is defined by a lag phase, an exponential polymerization phase, and a plateau, and can be followed using ThT fluorescence. The C-terminal peptide exhibited a conventional lag and exponential phase (TEM revealed few aggregates at Time 0; Fig. S2), but instead of plateauing, fluorescence dropped markedly at 96 h. This drop in fluorescence appeared to be due to changes in the amyloid fiber organization, involving a transition from a fiber "network" at 72 h, to short, thick fiber aggregates at 96 h (Fig. 3, Fig. S2). In contrast, the N-terminal peptide, formed amyloid fibers that bundled together though lateral associations, and exhibited a two-stage lag and exponential phase. Unlike either individual domain, the full length ChpH peptide lacked an obvious lag in its polymerization. While the absence of a lag phase could suggest that fiber formation was nucleation-independent, TEM images taken at "Time 0" for this peptide show that there are small aggregates in the sample (Fig. S2); it is possible that these could promote ChpH polymerization and eliminate any lag phase. Seeding experiments revealed that ChpH fiber formation could be accelerated in the presence of existing fiber seeds (particularly those of the N terminus), suggesting that its polymerization may be differentially responsive to different amyloids. Notably, the full length ChpH peptide polymerized much more rapidly than either the N- or C-terminal peptides (on the order of days), suggesting that these two domains may make synergistic contributions to the polymerization process. Rapid polymerization could be important to prevent unwanted accumulation of intermediate species during amyloidogenesis, complexes that some propose to be the primary source of amyloid-related cytotoxicity (32, 33).

Amyloid domains of different proteins do not share extensive sequence conservation, although many amyloids share common characteristics. For example, glutamine/asparagine-rich sequences are found in diverse amyloids, as are hydrophobic-rich sequences (34–36). The C-terminal ChpH amyloid domain is extremely hydrophobic, and this likely contributes to its aggregation propensity. The specific sequence within this amyloid domain is, however, critically important for effective polymerization, as single aa substitutions that did not dramatically alter the hydrophobicity profile (Table S1), led to peptides that were impaired in their amyloid polymerization, and proteins that were defective in promoting aerial development. We compared the ChpH amyloid domain sequences to the other chaplins in *S. coelicolor*, and found the N-terminal domain to be identical in ChpF and G, while in ChpD, a single conservative substitution was found (Val to Ile) (Fig. S7). ChpE differed at three of the 10 positions. Within the C terminus, the VIGLL sequence was conserved in ChpD, F, and G (ChpE has VIGVL), although the preceding Ser residue was unique to ChpH, and is conserved in 19/20 ChpH sequences from different *Streptomyces* species; other short chaplins have Asp or Asn in place of Ser. Changing this residue to an Ala (or Asp; Fig. S8) in ChpH adversely affected aerial hyphae formation, suggesting that this residue may define specific activities of different chaplin proteins.

Collectively, our studies have defined two distinct amyloid domains within the chaplin proteins, and have separated the contributions made by each domain to the function of the mature protein.

Materials and Methods

Bacterial Strains, Plasmids, and Growth Conditions. *S. coelicolor* strain J3149A (10) was used in constructing the different minimal chaplin strains. Strains were cultured at 30 °C on mannitol soy flour (MS) agar medium. *E. coli* DH5α (37) (plasmid construction), and ET12567/pUZ8002 (38, 39) (generating methylation-free DNA and conjugating plasmid DNA into *S. coelicolor*) were grown at 37 °C in Luria Bertani media. Plasmids are listed in Table S2. Plasmid conjugations were conducted as described previously (40).

***chpH* Mutagenesis.** *chpH* was excised from pIJ6935 (11) using EcoRI and ligated into EcoRI-digested pIJ2925 (41). The *chpH*-pIJ2925 plasmid served as template for site-directed mutagenesis using primers listed in Table S3 and as outlined previously (15). To replace the "VIGLL" sequence with five Ala residues, *chpH* was amplified as two halves using iProof DNA polymerase (BioRad) with M13 forward/VIGLL-AAAAA1 and M13 reverse/VIGLL-AAAAA2 primers (Table S3). The halves were then annealed together and amplified using M13 primers (Table S3). Mutations were confirmed by sequencing. Mutant (*chpH**) genes were excised using EcoRI and cloned into EcoRI-digested pIJ2925 containing *chpC*. *chpH**-*chpC* fragments were then excised with BglII, cloned into BamHI-digested pSET152 (42), and conjugated into *S. coelicolor* strain J3149A.

Construction of *chpH* Deletions. *chpH* deletions were generated by PCR-amplifying *chpH* from *chpH*-pIJ2925 as two halves. The 5′ sequence common to all three N-terminal deletions was amplified using the M13 reverse primer and ChpHdelRev (Table S3), while the 3′ sequence was amplified using the M13 forward primer and a *chpH*-specific primer that annealed immediately after the sequence to be deleted, and included a 5′ extension identical to the 3′ end of the first product. The two products were annealed together and amplified in a second reaction using the M13 primers. A similar strategy was used to remove the C-terminal VIGLL sequence, only using ChpHVIGLL1/M13 reverse and ChpHVIGLL2/M13 forward primers (Table S3). All mutant plasmids were sequenced to ensure that only the desired mutation was introduced. The *chpH* deletions were cloned upstream of *chpC* and introduced into *S. coelicolor* J3149A by conjugation.

Scanning Electron Microscopy. SEM was carried out as previously described (15, 43). Images were saved as TIF files and manipulated in Adobe Photoshop 8.0. Relative numbers of spore chains for wild type (WT) and mutant ChpH-expressing strains were determined by counting chains captured in at least five independent micrographs.

Isolation and Analysis of Chaplin Proteins. The chaplins were isolated from cell wall extracts and analyzed using MALDI-ToF mass spectrometry, as described previously (10).

Synthetic Peptide and Sonicated Seed Fibril Preparation. Lyophilized synthetic peptides (Proteintech Group Inc.) were suspended in trifluoroacetic acid (TFA) and water bath sonicated for 30 min. Aliquots of the peptide solution were then transferred to preweighed tubes and the TFA was evaporated. The tubes were reweighed to determine the dry peptide weight before being stored at −80 °C. To prepare amyloid seeds, 1 week-old fibers were sonicated using 3×15 sec bursts on ice, before immediately being added to peptide samples.

Thioflavin T Assay. Peptides were redissolved in ice-cold 50 mM KPi (pH 7.2) buffer at 0.5 mg/mL. At each time point, 98 μL of peptide was mixed with 2 μL 1 mM ThT in duplicate and deposited in the wells of a black, flat-bottom 96-well plate (Microfluor, Thermo Scientific). Plates were covered with ABsolute™ QPCR seal (Thermo Scientific) to prevent evaporation. Fluorescence was measured with a BioTek Synergy 4 microplate reader (Fisher Scientific) at 450 nm excitation and 490 nm emission.

Circular Dichroism Analysis. CD spectra were collected at the same time as the ThT assays were being performed, using the same peptide mixture. Peptides were diluted from 0.5 mg/mL to 0.25 mg/mL with ice-cold 50 mM KPi buffer (pH 7.2) (5 mg/mL samples were also tested for the C-terminal mutant peptides) and transferred to a 1-mm quartz cuvette. CD spectra of the buffer (no protein) were subtracted from peptide-containing solution values. Spectra were recorded from 190 to 260 nm using an Aviv 410 spectrometer.

Protease Resistance. Proteinase K (Roche) was added to two week-old fibers or freshly purified SCO3571 (Crp) (both 0.5 mg/mL) in 50 mM KPi buffer to a final concentration of 10 μg/mL. Samples were incubated at 37 °C and reactions were stopped by freezing at −80 °C. Samples were thawed immediately before analysis by CD spectroscopy.

Transmission Electron Microscopy. Samples for electron microscopy were prepared on freshly made continuous carbon grids with a previous glow-discharge treatment of 10 sec. Grids were floated on a 5 μL drop of peptide solution (0.5 or 5 mg/mL) for 2 min. Excess sample was blotted and the grids were stained with 2% Phosphotungstic acid (PTA) solution (Canemco and Marivac Inc.) for 1 min. The 2% PTA solution was prepared in water and the final pH of the solution was adjusted with 5 M sodium hydroxide to pH 7.0. The stain solution was filtered with Acrodisc 25 mm syringe filter with 0.2 μM Supor Membrane (PALL Corporation) before use. Specimens were imaged at a nominal magnification of 75,000× or 120,000× in a JEOL 1200-EX electron microscope operated at 80 kV. All images were acquired on AMT XR-41 Side-Mount Cooled 4 megapixel format CCD camera.

ACKNOWLEDGMENTS. We thank Drs. Raquel and Richard Epand for their assistance with the circular dichoism spectroscopy, Kim Findlay and Marcia Reid for assistance with the scanning electron microscopy, Chan Gao for provision of SCO3571 protein, and Marin Franchetto for technical assistance. This work was supported by the Canada Research Chairs program (to M.A.E.), and a grant from the Canadian Institutes for Health Research (to M.A.E.; grant no. MOP-93635).

1. Chiti F, Dobson CM (2006) Protein misfolding, functional amyloid, and human disease. *Annu Rev Biochem* 75:333–366.
2. Bieler S, et al. (2005) Amyloid formation modulates the biological activity of a bacterial protein. *J Biol Chem* 280:26880–26885.
3. Oh J, et al. (2007) Amyloidogenesis of type III-dependent harpins from plant pathogenic bacteria. *J Biol Chem* 282:13601–13609.
4. Alteri CJ, et al. (2007) *Mycobacterium tuberculosis* produces pili during human infection. *Proc Natl Acad Sci USA* 104:5145–5150.
5. Romero D, Aguilar C, Losick R, Kolter R (2010) Amyloid fibers provide structural integrity to *Bacillus subtilis* biofilms. *Proc Natl Acad Sci USA* 107:2230–2234.
6. Hardy GG, et al. (2010) A localized multimeric anchor attaches the *Caulobacter* holdfast to the cell pole. *Mol Microbiol* 76:409–427.
7. Dueholm MS, et al. (2010) Functional amyloid in *Pseudomonas*. *Mol Microbiol* 77:1009–1020.
8. Barnhart MM, Chapman MR (2006) Curli biogenesis and function. *Annu Rev Microbiol* 60:131–147.
9. de Jong W, Wosten HA, Dijkhuizen L, Claessen D (2009) Attachment of *Streptomyces coelicolor* is mediated by amyloidal fimbriae that are anchored to the cell surface via cellulose. *Mol Microbiol* 73:1128–1140.
10. Capstick DS, Willey JM, Buttner MJ, Elliot MA (2007) SapB and the chaplins: connections between morphogenetic proteins in *Streptomyces coelicolor*. *Mol Microbiol* 64:602–613.
11. Elliot MA, et al. (2003) The chaplins: a family of hydrophobic cell-surface proteins involved in aerial mycelium formation in *Streptomyces coelicolor*. *Genes Dev* 17:1727–1740.
12. Claessen D, et al. (2003) A novel class of secreted hydrophobic proteins is involved in aerial hyphae formation in *Streptomyces coelicolor* by forming amyloid-like fibrils. *Genes Dev* 17:1714–1726.
13. Elliot MA, Buttner MJ, Nodwell JR (2007) Multicellular development in *Streptomyces*. *Myxobacteria: Multicellularity and Differentiation*, ed DE Whitworth (American Society for Microbiology Press, Washington, DC), pp 419–438.
14. Willey JM, Willems A, Kodani S, Nodwell JR (2006) Morphogenetic surfactants and their role in the formation of aerial hyphae in *Streptomyces coelicolor*. *Mol Microbiol* 59:731–742.
15. Di Berardo C, et al. (2008) Function and redundancy of the chaplin cell surface proteins in aerial hypha formation, rodlet assembly, and viability in *Streptomyces coelicolor*. *J Bacteriol* 190:5879–5889.
16. Claessen D, et al. (2004) The formation of the rodlet layer of streptomycetes is the result of the interplay between rodlins and chaplins. *Mol Microbiol* 53:433–443.
17. Claessen D, et al. (2002) Two novel homologous proteins of *Streptomyces coelicolor* and *Streptomyces lividans* are involved in the formation of the rodlet layer and mediate attachment to a hydrophobic surface. *Mol Microbiol* 44:1483–1492.
18. Esteras-Chopo A, Serrano L, Lopez de la Paz M (2005) The amyloid stretch hypothesis: recruiting proteins toward the dark side. *Proc Natl Acad Sci USA* 102:16672–16677.
19. Pastor MT, Esteras-Chopo A, Serrano L (2007) Hacking the code of amyloid formation: the amyloid stretch hypothesis. *Prion* 1:9–14.
20. LeVine H, III (1999) Quantification of beta-sheet amyloid fibril structures with thioflavin T. *Methods Enzymol* 309:274–284.
21. Fernandez-Escamilla AM, Rousseau F, Schymkowitz J, Serrano L (2004) Prediction of sequence-dependent and mutational effects on the aggregation of peptides and proteins. *Nat Biotechnol* 22:1302–1306.
22. Conchillo-Sole O, et al. (2007) AGGRESCAN: a server for the prediction and evaluation of "hot spots" of aggregation in polypeptides. *BMC Bioinformatics* 8:65.
23. Garbuzynskiy SO, Lobanov MY, Galzitskaya OV (2010) FoldAmyloid: a method of prediction of amyloidogenic regions from protein sequence. *Bioinformatics* 26:326–332.
24. Bryson K, et al. (2005) Protein structure prediction servers at University College London. *Nucleic Acids Res* 33(Web Server issue):W36–38.
25. Cole C, Barber JD, Barton GJ (2008) The Jpred 3 secondary structure prediction server. *Nucleic Acids Res* 36(Web Server issue):W197–201.
26. Otzen D, Nielsen PH (2008) We find them here, we find them there: functional bacterial amyloid. *Cell Mol Life Sci* 65:910–927.
27. Wang X, Hammer ND, Chapman MR (2008) The molecular basis of functional bacterial amyloid polymerization and nucleation. *J Biol Chem* 283:21530–21539.
28. Wang X, Smith DR, Jones JW, Chapman MR (2007) In vitro polymerization of a functional *Escherichia coli* amyloid protein. *J Biol Chem* 282:3713–3719.
29. Westermark G, et al. (1999) Differences in amyloid deposition in islets of transgenic mice expressing human islet amyloid polypeptide versus human islets implanted into nude mice. *Metabolism* 48:448–454.
30. Nilsson MR, Raleigh DP (1999) Analysis of amylin cleavage products provides new insights into the amyloidogenic region of human amylin. *J Mol Biol* 294:1375–1385.
31. Jaikaran ET, et al. (2001) Identification of a novel human islet amyloid polypeptide beta-sheet domain and factors influencing fibrillogenesis. *J Mol Biol* 308:515–525.
32. Bucciantini M, et al. (2002) Inherent toxicity of aggregates implies a common mechanism for protein misfolding diseases. *Nature* 416:507–511.
33. Caughey B, Lansbury PT (2003) Protofibrils, pores, fibrils, and neurodegeneration: separating the responsible protein aggregates from the innocent bystanders. *Annu Rev Neurosci* 26:267–298.
34. Kim W, Hecht MH (2006) Generic hydrophobic residues are sufficient to promote aggregation of the Alzheimer's Abeta42 peptide. *Proc Natl Acad Sci USA* 103:15824–15829.
35. DePace AH, Santoso A, Hillner P, Weissman JS (1998) A critical role for amino-terminal glutamine/asparagine repeats in the formation and propagation of a yeast prion. *Cell* 93:1241–1252.
36. Michelitsch MD, Weissman JS (2000) A census of glutamine/asparagine-rich regions: implications for their conserved function and the prediction of novel prions. *Proc Natl Acad Sci USA* 97:11910–11915.
37. Hanahan D (1983) Studies on transformation of *Escherichia coli* with plasmids. *J Mol Biol* 166:557–580.
38. MacNeil DJ, et al. (1992) Analysis of *Streptomyces avermitilis* genes required for avermectin biosynthesis utilizing a novel integration vector. *Gene* 111:61–68.
39. Paget MS, Chamberlin L, Atrih A, Foster SJ, Buttner MJ (1999) Evidence that the extracytoplasmic function sigma factor sigmaE is required for normal cell wall structure in *Streptomyces coelicolor* A3(2). *J Bacteriol* 181:204–211.
40. Kieser T, Bibb MJ, Buttner MJ, Chater KF, Hopwood DA (2000) *Practical Streptomyces genetics* (The John Innes Foundation, Norwich, United Kingdom).
41. Janssen GR, Bibb MJ (1993) Derivatives of pUC18 that have BglII sites flanking a modified multiple cloning site and that retain the ability to identify recombinant clones by visual screening of *Escherichia coli* colonies. *Gene* 124:133–134.
42. Bierman M, et al. (1992) Plasmid cloning vectors for the conjugal transfer of DNA from *Escherichia coli* to *Streptomyces* spp. *Gene* 116:43–49.
43. Haiser HJ, Yousef MR, Elliot MA (2009) Cell wall hydrolases affect germination, vegetative growth, and sporulation in *Streptomyces coelicolor*. *J Bacteriol* 191:6501–6512.

Supporting Information

Capstick et al. 10.1073/pnas.1018715108

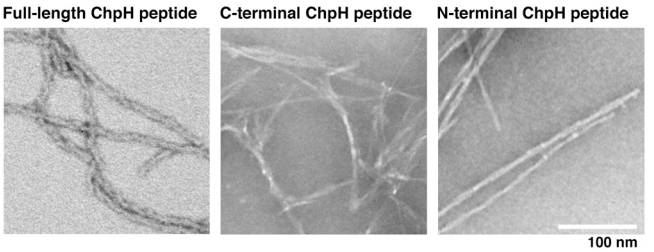

Fig. S1. Comparison of full length ChpH, N- and C-terminal fiber morphologies. Close-up view of negatively stained full length, C-terminal and N-terminal ChpH peptides (0.5 mg/mL) after 120 h, 72 h, and 120 h of incubation at room temperature, respectively.

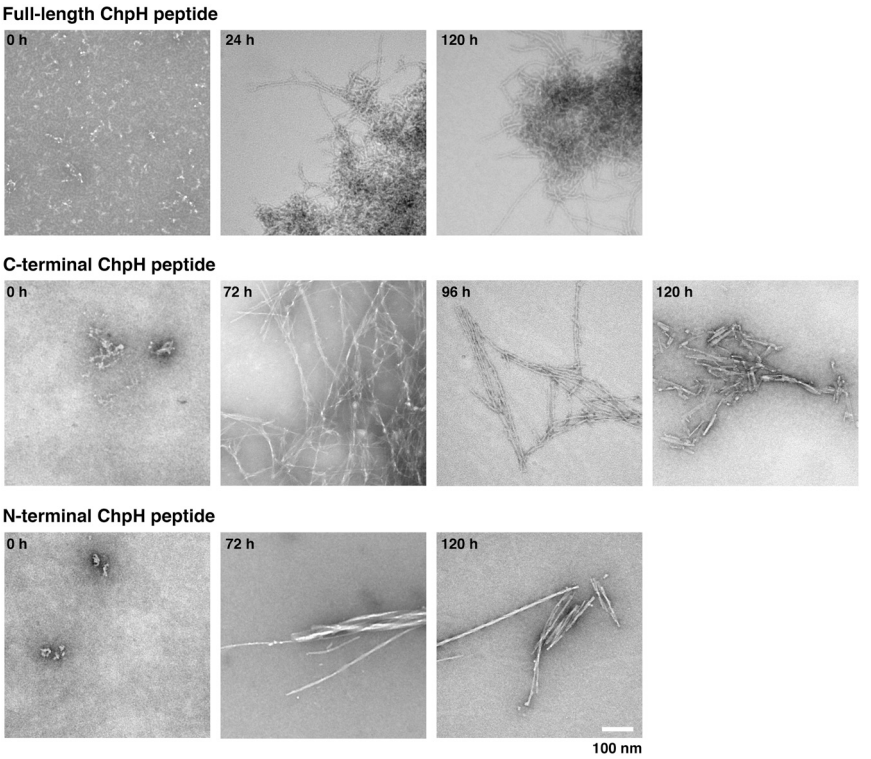

Fig. S2. Time course of negatively stained electron micrographs of the full length ChpH peptide (top row), C-terminal ChpH peptide (center row) and N-terminal peptide (bottom row). Images of peptides (0.5 mg/mL) were captured following incubation at room temperature for the times indicated.

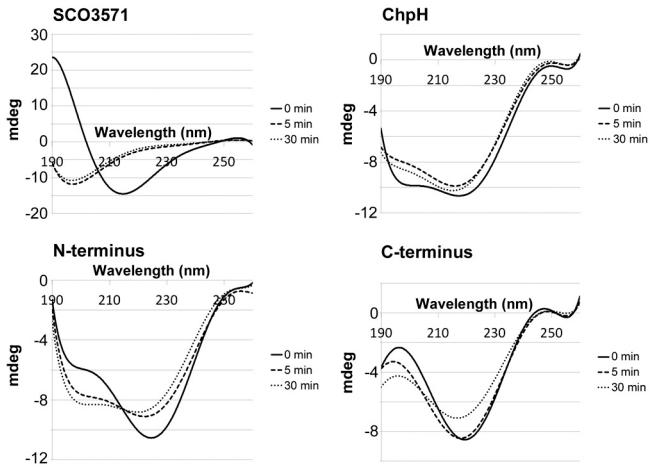

Fig. S3. Proteinase K (10 μg/mL) was added to 0.5 mg/mL preparations of: SCO3571 (a nonamyloid transcription factor from *Streptomyces coelicolor*) (top left) or two week old fibers of ChpH (top right), N-terminal ChpH (bottom left) and C-terminal ChpH (bottom right). Within 5 min of protease treatment, SCO3571 was completely unstructured (as indicated by the pronounced minimum at 200 nm), while the ChpH-derived fibers all retained structure (specifically, β-rich structure), even after 30 min of protease exposure.

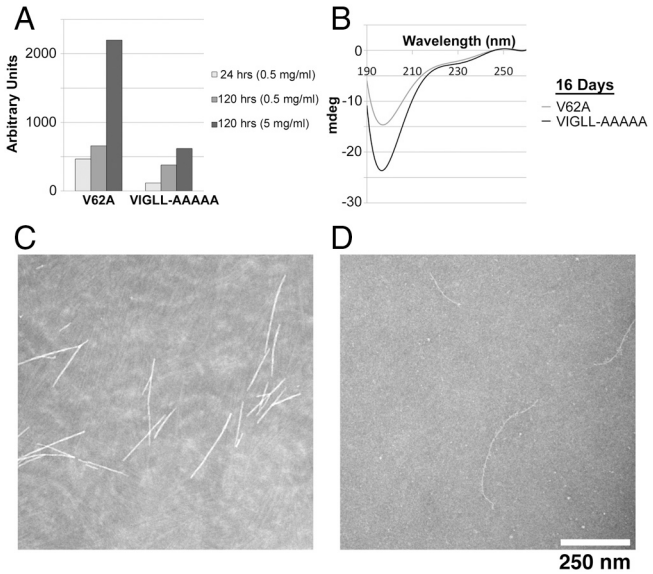

Fig. S4. Analysis of the C-terminal ChpH V62A (GNTIS**A**IGLLNPAFGN) and VIGLL-AAAAA (GNTIS**AAAAA**NPAFGN) mutant peptides in vitro. (*A*) ThT fluorescence of the two mutant peptides (incubated at 0.5 mg/mL or 5 mg/mL) after 24 and 120 h. Mutant peptides incubated at 5 mg/mL were diluted to 0.5 mg/mL with buffer before measurements were taken. (*B*) Secondary structure analysis of the mutant peptides (0.5 mg/mL) using CD spectroscopy after 16 d. Peptides were diluted to 0.25 mg/mL for CD measurements. (*C*) and (*D*) Negative stained EMs of (*C*) V62A and (*D*) VIGLL-AAAAA mutant C-terminal ChpH peptides (5 mg/mL) collected after 5 d of incubation at room temperature.

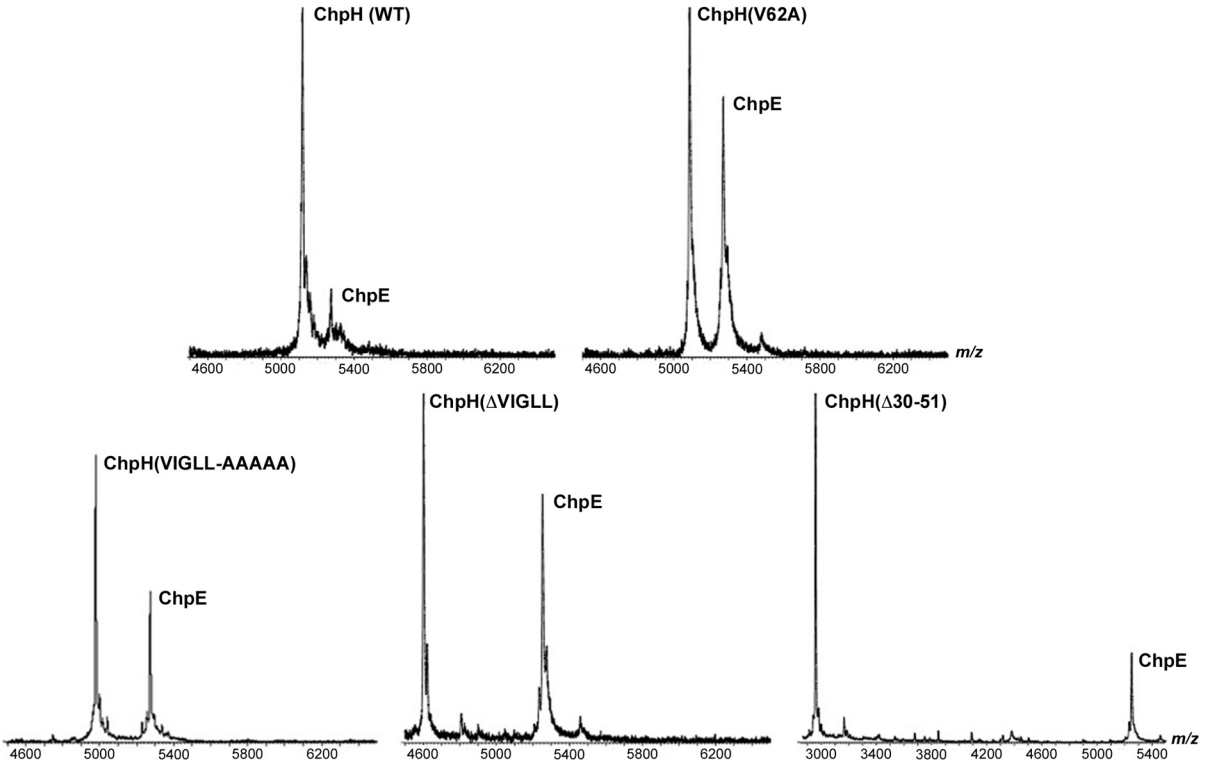

Fig. S5. MALDI-ToF mass spectrometry of cell wall extracts from a selection of ChpH mutants and a strain producing wild type ChpH (WT) grown for 7 d on mannitol soy flour (MS) medium. Peaks corresponding to ChpH and ChpE are labeled. The *x*-axis represents the mass (m)/charge (z) ratio, where $z = 1$. Note that relative ChpH and ChpE levels vary between different preparations [see (1); (2); (3)]; the one consistent observation is that ChpH levels are always greater than ChpE levels in wild type strains when detected using MALDI-ToF mass spectrometry.

1 Elliot MA, et al. (2007) The chaplins: a family of hydrophobic cell-surface proteins involved in aerial mycelium formation in *Streptomyces coelicolor*. *Genes Dev* 17:1727–1740.
2 Claessen D, et al. (2003) A novel class of secreted hydrophobic proteins is involved in aerial hyphae formation in *Streptomyces coelicolor* by forming amyloid-like fibrils. *Genes Dev* 17:1714–1726.
3 Capstick DS, et al. (2007) SapB and the chaplins: connections between morphogenetic proteins in *Streptomyces coelicolor*. *Mol Microbiol* 64:602–613.

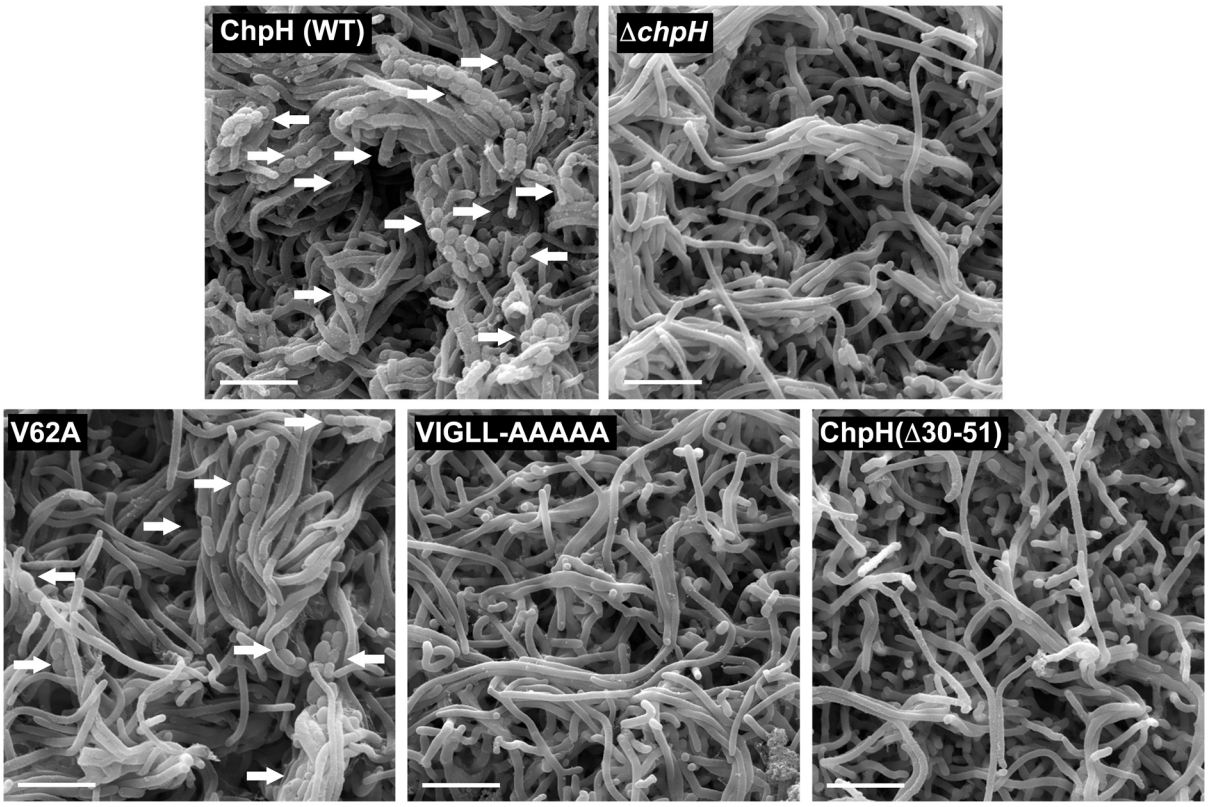

Fig. S6. The phenotypic effect of ChpH mutations on aerial development, compared to a strain producing wild type ChpH (WT) and a strain completely lacking ChpH (Δ*chpH*) after growth for 12 d on MS medium. Spore chains are indicated with arrows. (Scale bars, 5 μm).

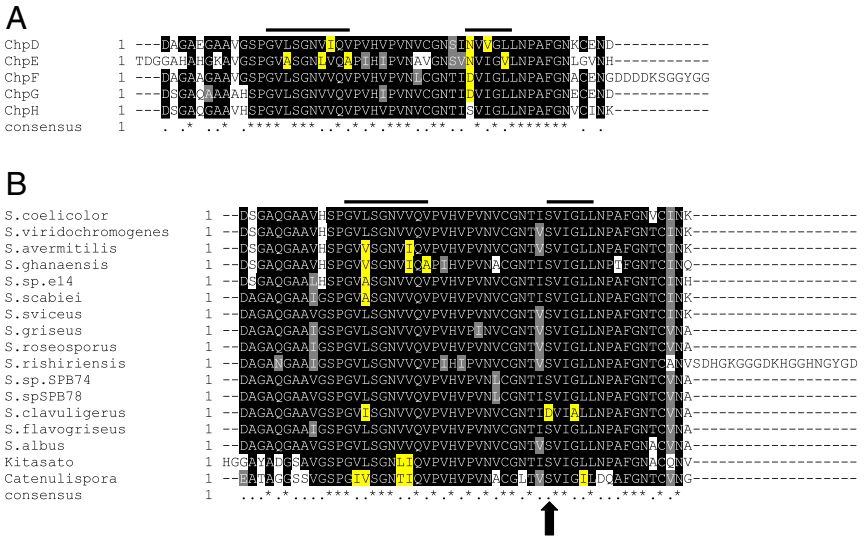

Fig. S7. Alignment of mature chaplin sequences. (*A*) Mature short chaplins from *S. coelicolor*, with black bars above the alignment indicating the amyloid domains, and residues highlighted in yellow indicating deviations relative to the ChpH sequence. (*B*) Mature ChpH sequences from diverse actinomycetes (the *chpH* designation requiring genetic synteny), with black bars above the alignment indicating the amyloid domains, residues highlighted in yellow indicating deviations from the ChpH (*S. coelicolor*) sequence, and the arrow indicating the highly conserved Ser residue that is specific to ChpH sequences.

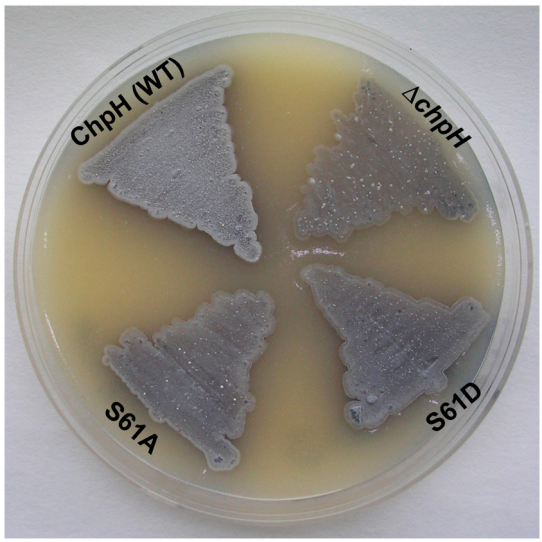

Fig. S8. Four day cultures grown on MS medium, expressing wild type ChpH (WT), lacking *chpH* (Δ*chpH*), and expressing ChpH with either an Ala or Asp residue substituted for Ser61.

Table S1. Hydrophobicity scores for ChpH mutants

Chaplin	Hydrophobicity (GRAVY*)
ChpH (WT)	0.6
I60A	0.548
S61A	0.65
V62A	0.554
I63A	0.548
G54A	0.642
L55A	0.562
L56A	0.562
V72A	0.554
VIGLL-AAAAA	0.467
ΔVIGLL	0.326
ΔN6	0.663
ΔN12	0.653
ΔN22	0.577

*GRAVY: Grand average of hydropathicity index (the higher the positive number, the more hydrophobic the protein sequence) (1).

1 Kyte J, Doolittle RF (1982) A simple method for displaying the hydropathic character of a protein. *J Mol Biol* 157:105–132.

Table S2. Plasmids used in this study

Plasmid	Description	Reference
pIJ2925	*E. coli* cloning vector	(1)
pSET152	Integrative cloning vector	(2)
pIJ6935	pSET152 + *chpHC*	(3)
pMC102	pIJ2925 + *chpH*	This work
pMC103	pSET152 + Δ*chpH-chpC*	This work
pMC104	pSET152 + *chpH*(I60A)-*chpC*	This work
pMC105	pSET152 + *chpH*(S61A)-*chpC*	This work
pMC106	pSET152 + *chpH*(S61D)-*chpC*	This work
pMC107	pSET152 + *chpH*(V62A)-*chpC*	This work
pMC108	pSET152 + *chpH*(I63A)-*chpC*	This work
pMC109	pSET152 + *chpH*(G64A)-*chpC*	This work
pMC110	pSET152 + *chpH*(L65A)-*chpC*	This work
pMC111	pSET152 + *chpH*(L66A)-*chpC*	This work
pMC112	pSET152 + *chpH*(V73A)-*chpC*	This work
pMC113	pSET152 + *chpH*(VIGLL-AAAAA)-*chpC*	This work
pMC114	pSET152 + *chpH*(ΔVIGLL)-*chpC*	This work
pMC115	pSET152 + *chpH*(Δ30-35)-*chpC*	This work
pMC116	pSET152 + *chpH*(Δ30-41)-*chpC*	This work
pMC117	pSET152 + *chpH*(Δ30-51)-*chpC*	This work

1 Janssen GR, Bibb MJ (1993) Derivatives of pUC18 that have BglII sites flanking a modified multiple cloning site and that retain the ability to identify recombinant clones by visual screening of *Escherichia coli* colonies. *Gene* 124:133–134.

2 Bierman M, et al. (1992) Plasmid cloning vectors for the conjugal transfer of DNA from *Escherichia coli* to *Streptomyces* spp. *Gene* 116:43–49.

3 Elliot MA, et al. (2007) The chaplins: a family of hydrophobic cell-surface proteins involved in aerial mycelium formation in *Streptomyces coelicolor*. *Genes Dev* 17:1727–1740.

Table S3. Oligonucleotide primers used in this study

Name	Sequence (5′ to 3′)	Use
I52.17c up	CGGAGTGGACGAGCGGGTGC	Cloning of Δ*chpH-chpC*
16c end	CGAGTACGGACACTGGGAG	Cloning of Δ*chpH-chpC*
I60A1	GTCTGCGGCAACACGGCCTCCGTGATCGGTCT	I60A mutagenesis
I60A2	AGACCGATCACGGAGGCCGTGTTGCCGCAGAC	I60A mutagenesis
S61A1	GCGGCAACACGATCGCCGTGATCGGTCTG	S61A mutagenesis
S61A2	CAGACCGATCACGGCGATCGTGTTGCCGC	S61A mutagenesis
S61D1	CTGCGGCAACACGATCGACGTGATCGGTCTGCTG	S61D mutagenesis
S61D2	CAGCAGACCGATCACGTCGATCGTGTTGCCGCAG	S61D mutagenesis
V62AFwd	AACACGATCTCCGCGATCGGTCTGCTGA	V62A mutagenesis
V62ARvs	TCAGCAGACCGATCGCGGAGATCGTGTT	V62A mutagenesis
I63AFwd	CACGATCTCCGTGGCCGGTCTGCTGAACCC	I63A mutagenesis
I63ARvs	GGGTTCAGCAGACCGGCCACGGAGATCGTG	I63A mutagenesis
G64AFwd	GATCTCCGTGATCGCTCTGCTGAACCCCG	G64A mutagenesis
G64ARvs	CGGGGTTCAGCAGAGCGATCACGGACATC	G64A mutagenesis
L65A1	GATCTCCGTGATCGGTGCGCTGAACCCCGCC	L65A mutagenesis
L65A2	GGCGGGGTTCAGCGCACCGATCACGGAGATC	L65A mutagenesis
L66A1	CCGTGATCGGTCTGGCGAACCCCGCCTTCG	L66A mutagenesis
L66A2	CGAAGGCGGGGTTCGCCAGACCGATCACGG	L66A mutagenesis
V73A1	CCGCCTTCGGCAACGCCTGCATCAACAAGTG	V73A mutagenesis
V73A2	CACTTGTTGATGCAGGCGTTGCCGAAGGCGG	V73A mutagenesis
VIGLL-AAAAA-1	GGCAACACGATCTCCGCGGCCGCTGCGGCGAACCCCGCCTTCGGCAAC	VIGLL/AAAAA mutagenesis
VIGLL-AAAAA-2	GTTGCCGAAGGCGGGGTTCGCCGCAGCGGCCGCGGAGATCGTGTTGCC	VIGLL-AAAAA mutagenesis
ChpHVIGLL1	GGAGATCGTGTTGCCGCAGA	VIGLL deletion
ChpHVIGLL2	TGCGGCAACACGATCTCCAACCCCGCCTTCGGCAACGT	VIGLL deletion
ChpHdelRev	GGCACCGGAGTCGGCGACGG	ChpH N-terminal deletions
ChpHdelFwd1	GTCGCCGACTCCGGTGCCTCGCCCGGCGTCCTTTCCGG	aa 30-35 deletion
ChpHdelFwd2	GTCGCCGACTCCGGTGCCGGCAACGTCGTTCAGGTTCC	aa 30-41 deletion
ChpHdelFwd3	GTCGCCGACTCCGGTGCCCCGGTGAACGTCTGCGGCAA	aa 30-51 deletion
M13 Fwd	CGCCAGGGTTTTCCCAGTCACG	Cloning and sequencing
M13 Rev	GCGGATAACAATTTCACACAGG	Cloning and sequencing